Supporting Information

High-Performance Semitransparent Organic Solar Cells Enabled by Pseudo-Planar Heterojunction Structures Combined with Optical Engineering

Ding Yang,[a] Rui Zhang,*[b] Yu Shi, [a] Xia Guo*[a] and Maojie Zhang*[a]

[a]Laboratory of Advanced Optoelectronic Materials, Suzhou Key Laboratory of Novel Semiconductor-optoelectronics Materials and Devices, College of Chemistry, Chemical Engineering and Materials Science, Soochow University, Suzhou 215123, China

E-mail: mjzhang@sdu.edu.cn; guoxia0610@sdu.edu.cn

[b]Department of Physics, Chemistry and Biology (IFM), Linköping University, Linköping, Sweden

E-mail: rui.zhang@liu.se

Materials

All chemicals and solvents were reagent grades and purchased from Damas-beta, Acros Organics, and Sigma-Aldrich. PM6 and BTP-eC9 were purchased from Solarmer Materials Inc.

Experimental Section

Transmission spectra and UV-vis-NIR absorption spectra Measurements

The transmission spectra and ultraviolet-visible-near infrared (UV-Vis-NIR) absorption spectra were taken on an Agilent Technologies Cary 5000 Series UV-Vis-NIR Spectrophotometer.

Calculation method of AVT

The average visible transmittance (AVT) is calculated according to the equation:

$$\mathrm{AVT} = \frac{\int T(\lambda) \times P(\lambda) \times S(\lambda)\, d(\lambda)}{\int P(\lambda) \times S(\lambda)\, d(\lambda)}$$

Where λ is the wavelength, T is the transmission, P is the normalized photopic spectral response of the eye, and S is the solar irradiance.

TOF-SIMS measurement

The time-of-flight secondary ion mass spectrometry (TOF-SIMS) used Cs^+ as the sputter source with energy of 500 eV and current of 40 nA. And the typical sputter area was 200 μm by 200 μm.

Contact angle measurement

The contact angle tests were performed on a Dataphysics OCA40 Micro surface contact angle analyzer. The surface energy of the polymers was characterized and calculated by the contact angles of the two probe liquids (ultrapure water and diiodomethane) with

the Owens and Wendt equation: $\gamma_{LV}(1 + \cos\theta) = 2(\gamma_S^d\gamma_L^d)^{1/2} + 2(\gamma_S^p\gamma_L^p)^{1/2}$, where γ_S and γ_L are the surface energy of the sample and the probe liquid, respectively. The superscripts d and p refer to the dispersion and polar components of the surface energy, respectively.

XPS measurement

X-ray photoelectron spectroscopy (XPS) was performed using a high-resolution X-ray photoelectron spectrometer (ULVAC, PHI Quantera SXM) and an Al X-ray source (1200 eV).

AFM and TEM measurements

Atomic force microscopy (AFM) measurement was obtained by using a Dimension 3100 (Veeco) Atomic Force Microscope in a tapping mode. Transmission electron microscopy (TEM) was performed on a Tecnai G2 F20 S-TWIN instrument at 200 kV accelerating voltage.

GIWAXS measurements

Grazing-incidence wide-angle X-ray scattering (GIWAXS) measurements were carried out with a Xeuss 3.0 SAXS/WAXS laboratory beamline, using a Cu X-ray source (1.54 Å) and a Pilatus3R 300K detector. The incidence angle is 0.2°.

***J-V* and EQE measurements**

The current density-voltage (*J-V*) characteristics of the OSCs were recorded with a keithley 2450. The power conversion efficiencies (PCEs) of the OSCs were measured under 1 sun, AM 1.5G (air mass 1.5 global) (100 mW cm^{-2}), using a SS-F5-3A (Enli Technology CO., Ltd.) solar simulator (AAA grade, 50 mm x 50 mm photo-beam size).

2×2 cm^2 monocrystalline silicon reference cell (SRC-00019, covered with a KG5 filter windows) was purchased from Enli Technology CO., Ltd. The external quantum efficiency (EQE) was measured by Solar Cell Spectral Response Measurement System QE-R3011 (Enli Technology CO., Ltd.). The light intensity at each wavelength was calibrated with a standard single-crystal Si photovoltaic cell.

TPC and TPV measurements

Transient photovoltage (TPV) and transient photocurrent (TPC) measurements were carried out under a 337 nm and 3.5 ns pulse laser (160 μJ per pulse at 10 Hz) and halide lamps (150 W). Voltage and current dynamics were recorded on a digital oscilloscope (Tektronix MDO3102).

SCLC measurements

The hole and electron mobilities of devices were evaluated from space-charge-limited current (SCLC) method with hole-only structure of ITO/PEDOT:PSS/active layer/MoO_3/Al and electron-only structure of ITO/ZnO/active layer/PFN-Br/Al, respectively. The corresponding charge mobilities are calculated from fitting the Mott-Gurney square law $J = 9\varepsilon_r\varepsilon_0\mu V^2/(8L^3)$, where J is the current density, ε_r is the dielectric permittivity of the active layer, ε_0 is the vacuum permittivity, L is the thickness of the active layer, μ is the hole or electron mobility.

Fabrication of organic solar cells.

The patterned indium tin oxide (ITO) coated glasses were cleaned by detergent and then underwent a wet-cleaning process inside an ultrasonic bath procedure, followed by ultrapure water, acetone and isopropanol in sequence and then placed in oven at 100 ^oC

for 10 min to remove the residual solvents. After the treatment in a UV-ozone cleaner for 20 min, PEDOT:PSS (Heraeus Clevios PVP Al 4083) was deposited by spin-coating under 6000 rpm for 40 s on the cleaned ITO substrates. Then the substrates were placed on a hot plate at 150 ^{o}C to anneal for 15 min and immediately transferred to a glove box. Opaque devices were fabricated with a structure of ITO/PEDOT:PSS/active layer/PFN-Br/Al. And semitransparent organic solar cells (ST-OSCs) were fabricated with a structure of ITO/PEDOT:PSS/active layer/PFN-Br/Au/Ag. For BHJ devices, donor (PM6) and acceptor (BTP-eC9) were co-dissolved in chloroform (CF) with D:A ratio of 1:1.2 at corresponding total concentrations of 18 mg mL^{-1}. The blend solutions were stirred for 4 hours under a temperature of 50 ^{o}C. Thereafter, the cooled blend solution was spin-coated at speed of 3500 rpm for 40 s to form the active layer, which were thermal annealing (TA) at 100 ^{o}C for 10 minutes. For PPHJ devices, the PM6 (12 mg mL^{-1}) was dissolved in chlorobenzene (CB) with 0.5 vol.% DIO, and BTP-eC9 (9 mg mL^{-1}) was dissolved in CF with 0.5 vol.% DIO.[1] Optimization of devices was performed via varying the spin-coating speed of each layers and TA conditions. And the best TA condition (80 ^{o}C, 5 min) was applied to the preparation of PPHJ ST-OSCs. PFN-Br layer was spin coated on the top of all the active layers at 2500 rpm for 30 s. Finally, for opaque devices, 100 nm Al layer was deposited by thermal evaporation through a defined shadow mask to determine the active area of the devices (~0.0265 cm^2) in a vacuum chamber (approximately 3×10^{-4} Pa). For ST-OSCs, 1 nm Au and 10 nm Ag layers were thermally deposited through a shadow mask.

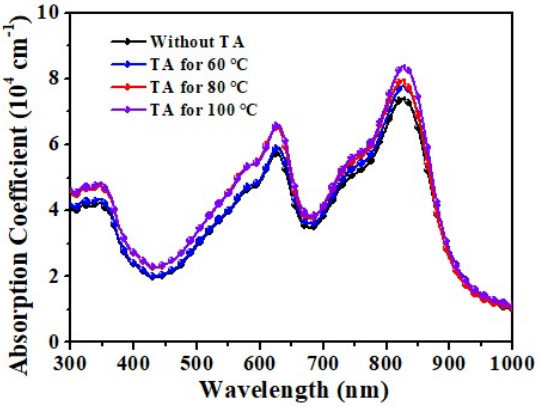

Fig. S1 Absorption coefficient spectra of PPHJ films with different TA temperatures.

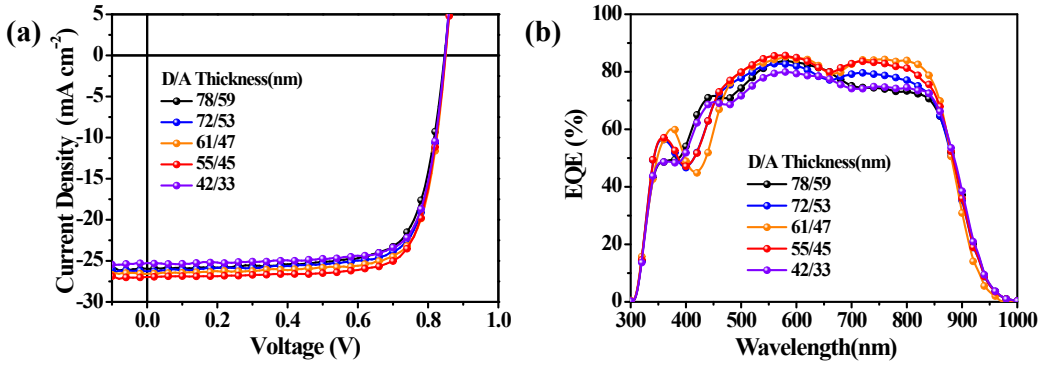

Fig. S2 (a) *J-V* curves and (b) EQE spectra of PPHJ OSCs with different D/A thicknesses.

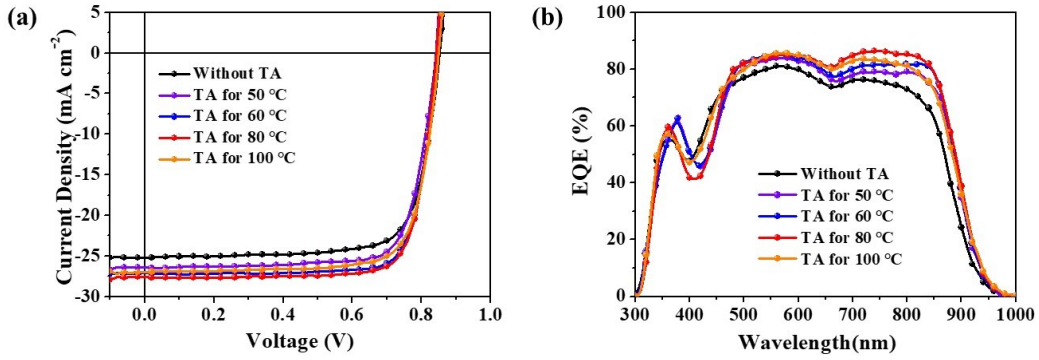

Fig. S3 (a) *J-V* curves and (b) EQE spectra of PPHJ OSCs with different annealing temperatures for 5 minutes.

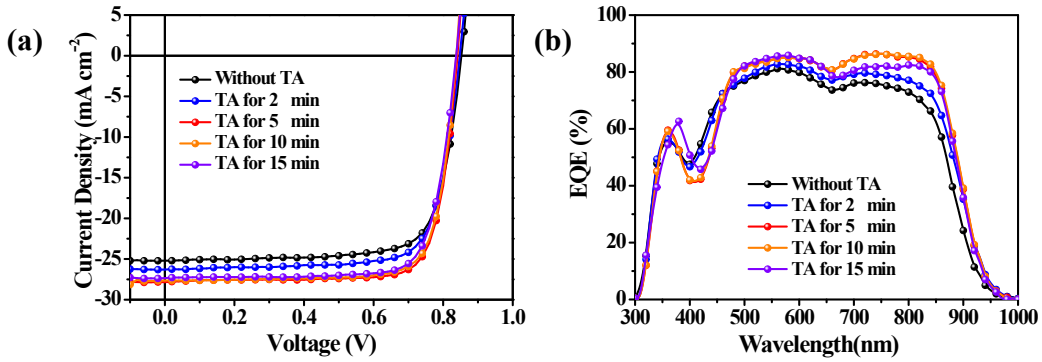

Fig. S4 (a) *J-V* curves and (b) EQE spectra of PPHJ OSCs with different annealing time at 80 °C.

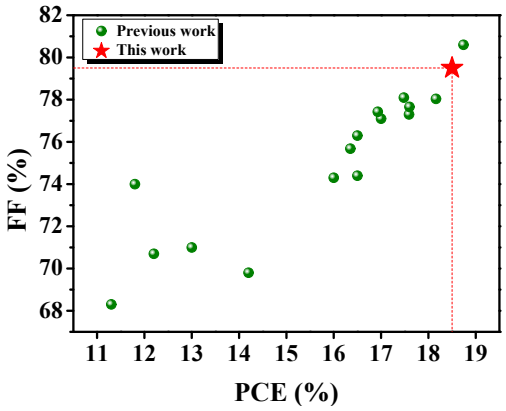

Fig. S5 Comparison of our results with previously reported FF and PCE for OSCs fabricated through sequential deposition method.

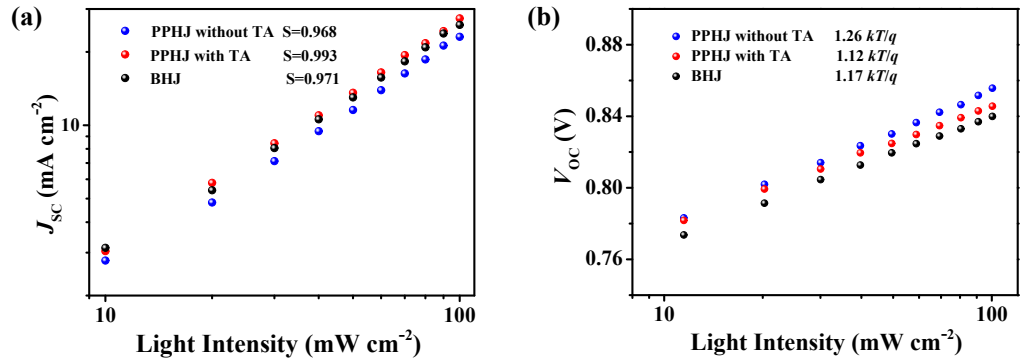

Fig. S6 P_{light}-dependent (a) J_{SC} and (b) V_{OC} curves of the PPHJ (without TA), PPHJ (with TA), and BHJ devices.

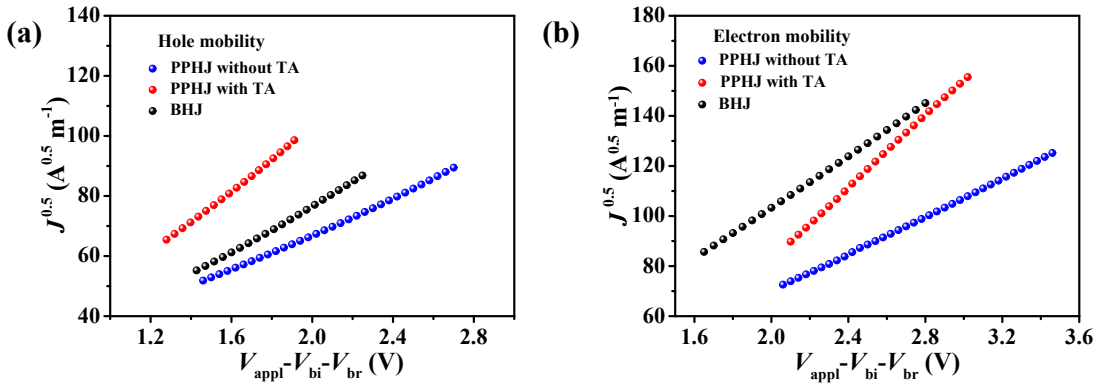

Fig. S7 $J^{0.5}$-V characteristics of (a) hole- and (b) electron-only devices based on the PPHJ (without TA), PPHJ (with TA), and BHJ films.

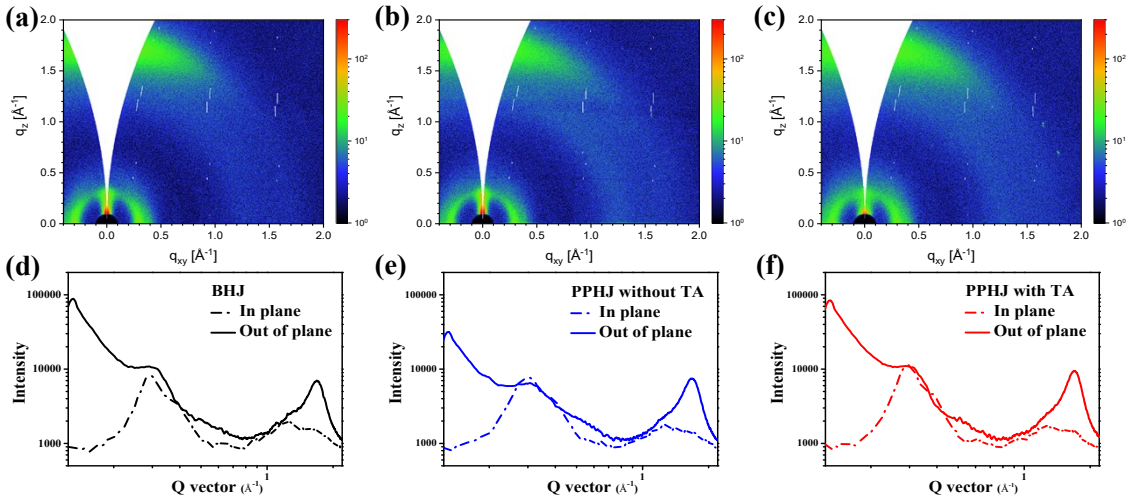

Fig. S8 (a-c) 2D GIWAXS images of BHJ, PPHJ (without TA), and PPHJ (with TA) films. (d-f) The corresponding out-of-plane (solid lines) and in-plane (dash lines) profiles.

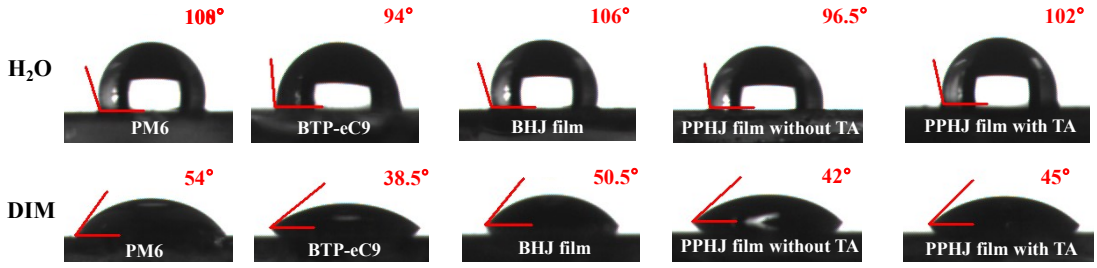

Fig. S9 Contact angle images of water and DIM droplets on PM6, BTP-eC9, BHJ, PPHJ (without TA), and PPHJ (with TA) films.

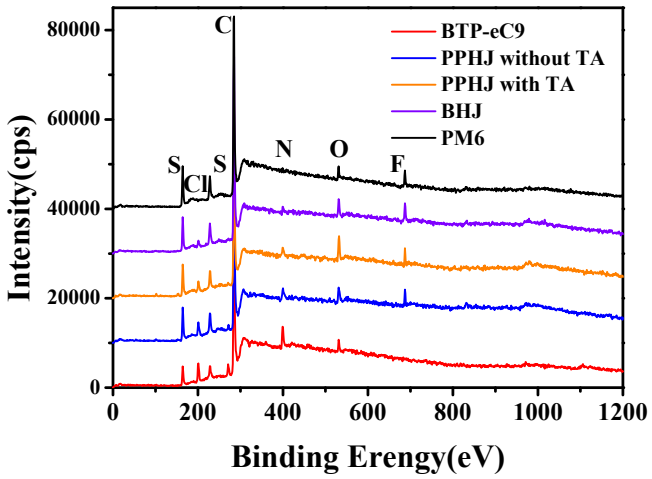

Fig. S10 XPS survey scans of PM6, BTP-eC9, BHJ, PPHJ (without TA), and PPHJ (with TA) films.

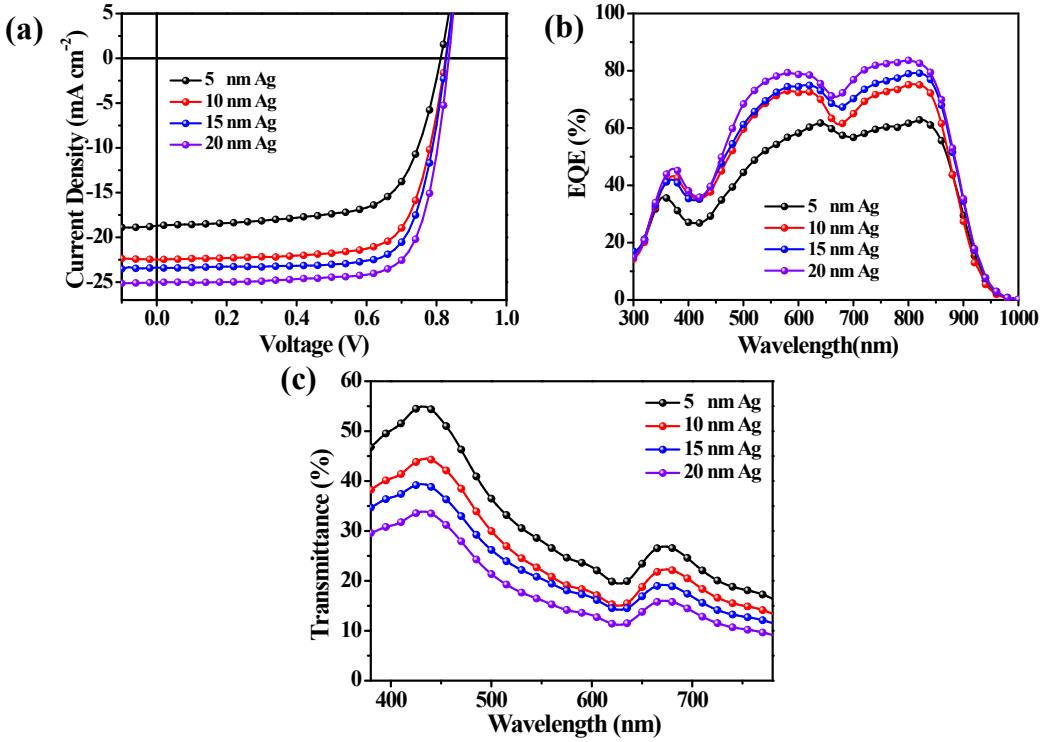

Fig. S11 (a) *J-V* curves, (b) EQE spectra and (c) transmittance spectra of ST-OSCs with different Ag electrode thicknesses.

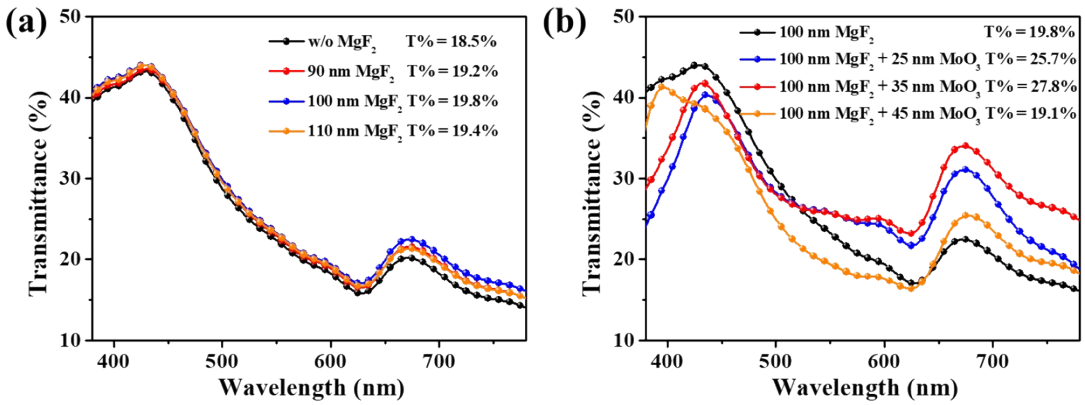

Fig. S12 Transmittance spectra of (a) ST-OSCs with different thicknesses MgF_2. (b) ST-OSCs with 100 nm MgF_2 and different thicknesses MoO_3.

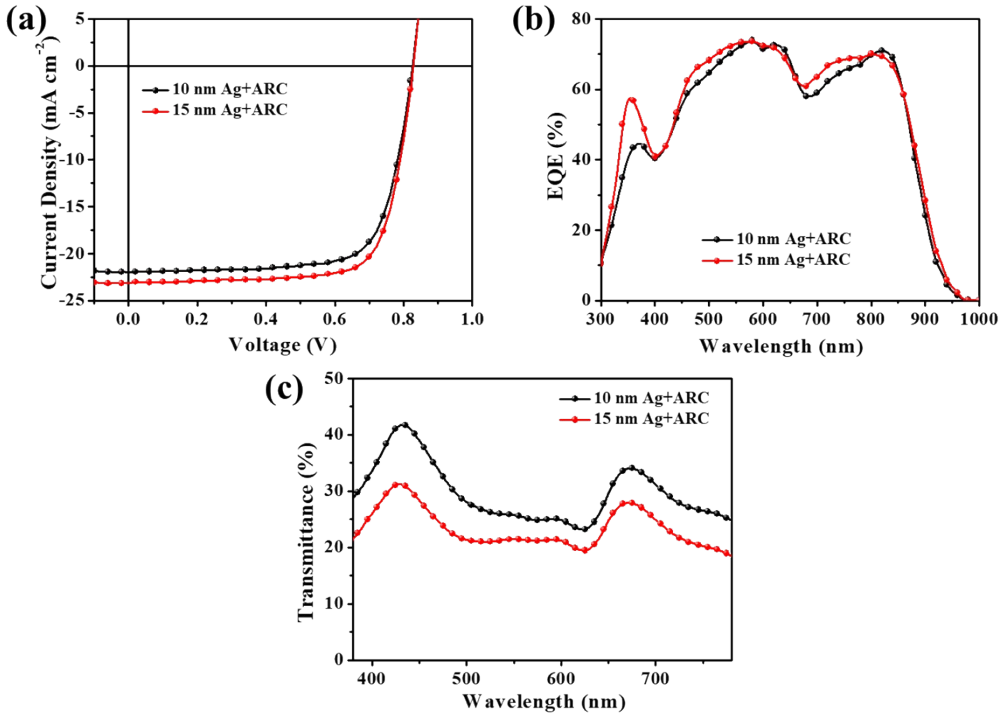

Fig. S13 (a) *J-V*, (c) EQE and (d) transmission curves of PPHJ ST-OSCs with different Ag electrode thicknesses and ARC layer.

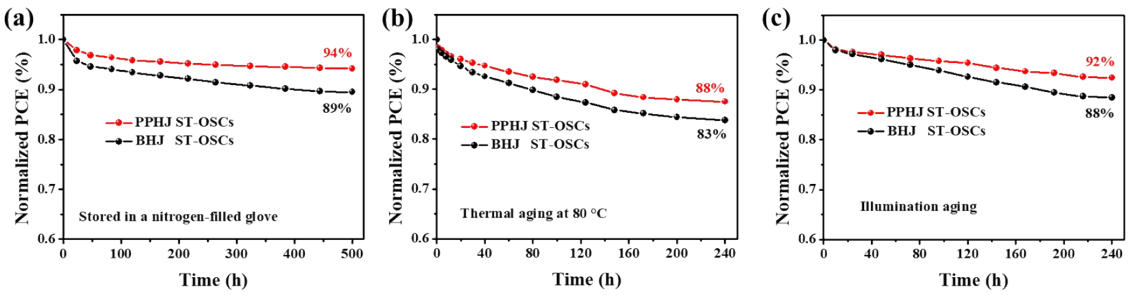

Fig. S14 (a) The storage stability, (b) thermal stability and (c) light-soaking stability of the PPHJ and BHJ ST-OSCs in a glovebox under nitrogen without encapsulation.

Table S1 Photovoltaic parameters for PPHJ OSCs with different PM6 and BTP-eC9 thicknesses. The active layers were annealed at 100 ℃ for 5 minutes.

PM6 (nm)	BTP-eC9 (nm)	V_{OC} (V)	J_{SC}/ J_{cal}[a] (mA cm^{-2})	FF (%)	PCE (%)
78	59	0.85	26.0/25.1	74.1	16.3
72	53	0.85	26.3/25.3	75.6	16.8
61	47	0.85	26.6/25.9	76.3	17.3
55	45	0.85	27.0/26.2	76.9	17.6
42	33	0.85	25.3/24.6	77.1	16.5

[a] Integrated J_{SC} is obtained from the EQE curve.

Table S2 Photovoltaic parameters of the PPHJ OSCs based on PM6/BTP-eC9 with thermal annealing for 5 minutes at different temperatures.

Condition	V_{OC} (V)	J_{SC}/ J_{cal}[a] (mA cm^{-2})	FF (%)	PCE (%)
w/o TA	0.85	25.3/24.5	75.4	16.2
TA for 50 °C	0.84	26.4/25.3	77.0	17.2
TA for 60 °C	0.84	27.1/26.1	79.9	18.2
TA for 80 °C	0.84	27.6/26.6	79.5	18.5
TA for 100 °C	0.85	27.0/26.2	76.9	17.6

[a] Integrated J_{SC} is obtained from the EQE curve.

Table S3 Photovoltaic parameters of the PPHJ OSCs based on PM6/BTP-eC9 with thermal annealing at 80 °C for different annealing time.

Condition	V_{OC} (V)	J_{SC}/ J_{cal}[a] (mA cm^{-2})	FF (%)	PCE (%)
w/o TA	0.85	25.3/24.5	75.4	16.2
TA for 2 min	0.85	26.3/25.3	76.0	17.0
TA for 5 min	0.84	27.6/26.6	79.5	18.5
TA for 10 min	0.84	27.6/26.6	78.7	18.2
TA for 15 min	0.84	27.3/26.3	78.1	17.9

[a] Integrated J_{SC} is obtained from the EQE curve.

Table S4 Photovoltaic paraments of OSCs based on sequential deposition method.

Active Layer	V_{OC} (V)	J_{SC} (mA cm^{-2})	FF (%)	PCE (%)	Ref.
PBDB-TFS1/IT-4F	0.90	20.3	71.0	13.0	2
PTFB-O/ITIC-Th	0.910	17.5	74.0	11.8	3
FTAZ/IT-M	0.958	18.6	70.7	12.2	4
PffBT4T2OD/IEICO-4F:FBR	0.74	22.4	68.3	11.3	5
PM6/IT-4F:F8IC	0.79	25.6	69.8	14.2	6
PM6/Y6	0.834	25.90	75.68	16.35	7

PT2/Y6	0.83	26.7	74.4	16.5	8
PM6/Y6	0.82	26.3	76.3	16.5	9
PM6/Y6:PCBM	0.83	26.6	77.1	17.0	10
PM6/Y6	0.85	25.51	77.43	16.93	11
PNTB6-Cl/N3	0.857	26.58	77.3	17.59	12
PM6/BTP-eC9	0.840	26.65	78.1	17.48	13
D18/BTIC-BO-4Cl	0.86	26.32	77.66	17.60	14
PM6/BO-4Cl:BTP-S2	0.861	27.14	78.04	18.16	13
PM6/L8-BO	0.89	26.11	80.6	18.74	15
PM6/BO-4F	0.82	26.2	74.3	16.0	16
PM6/BTP-eC9	0.84	27.6	79.5	18.5	This Work

Table S5 Extracted mobility of the hole and electron-only devices based on PPHJ (without TA), PPHJ (with TA) and BHJ films.

Device	μ_h ($cm^2 V^{-1} s^{-1}$)	μ_e ($cm^2 V^{-1} s^{-1}$)	μ_h/μ_e
PPHJ (w/o TA)	6.22×10^{-4}	5.02×10^{-4}	1.24
PPHJ (with TA)	8.33×10^{-4}	7.94×10^{-4}	1.05
BHJ	7.28×10^{-4}	6.28×10^{-4}	1.16

Table S6 The d-spacing and CCL of the (010) and (100) peaks of PPHJ (without TA), PPHJ (with TA) and BHJ films.

Sample	Out-of-plane			In-plane		
	π-π stacking (010)			Lamellar stacking (100)		
	q (Å^{-1})	d-spacing (Å)	CCL (Å)	q (Å^{-1})	d-spacing (Å)	CCL (Å)
BHJ	1.690	3.72	21.7	0.296	21.23	89.8
PPHJ (w/o TA)	1.682	3.74	21.2	0.294	21.37	75.7
PPHJ (with TA)	1.697	3.69	23.1	0.293	21.44	95.2

Table S7 Summary of contact angle (θ) and surface tension (γ) for neat PM6, neat BTP-eC9, BHJ, PPHJ (without TA), and PPHJ (with TA) films.

Sample	θ_{water} (°)	θ_{DIM} (°)	γ_d (mN m^{-1})	γ_p (mN m^{-1})	γ (mN m^{-1})
PM6	108	54	34.30	0.09	34.4
BTP-eC9	94	38.5	40.64	0.33	41.0
BHJ	106	50.5	36.22	0.06	36.3
PPHJ (w/o TA)	96.5	42	39.23	0.18	39.5
PPHJ (with TA)	102	45	38.85	0.00	38.8

Table S8 Atomic concentration of the top surface of neat PM6, neat BTP-eC9, BHJ, PPHJ (without TA), and PPHJ (with TA) films measured by XPS.

Sample	C (%)	S (%)	F (%)	N (%)	Cl (%)
PM6	86.6	10.9	2.5	0	0
BTP-eC9	83.1	4.6	0	8.1	4.2
BHJ	85.2	7.9	1.7	3.4	1.8
PPHJ (w/o TA)	84.1	5.5	1.2	5.9	3.3
PPHJ (with TA)	84.7	6.6	1.5	4.7	2.5

Table S9 Photovoltaic and optical parameters of PPHJ ST-OSCs with different Ag electrode thicknesses.

Ag Electrode Thickness(nm)	V_{OC} (V)	J_{SC}/ J_{cal}[a] (mA cm^{-2})	FF (%)	PCE (%)	AVT (%)	LUE (%)
20	0.83	24.8/24.1	76.5	15.7	13.5	2.12
15	0.83	23.4/22.6	75.1	14.6	16.8	2.45
10	0.82	22.5/21.8	72.1	13.3	18.5	2.46
5	0.81	18.7/17.8	67.4	10.2	23.2	2.36

[a] Integrated J_{SC} is obtained from the EQE curve.

Table S10 Photovoltaic and optical parameters of PPHJ ST-OSCs with different Ag electrode thicknesses and ARC layer.

Device	V_{OC} (V)	J_{SC} /J_{cal}[a] (mA cm^{-2})	FF (%)	PCE (%)	AVT (%)	LUE (%)
10 nm Ag + ARC	0.82	22.0/21.3	72.6	13.1	27.8	3.64
15 nm Ag + ARC	0.83	23.0/22.0	74.7	14.3	23.1	3.30

[a] Integrated J_{SC} is obtained from the EQE curve.

Table S11 Photovoltaic and optical parameters of the ST-OSCs with AVT over 25% in literatures reported in recent five years.

Active Layer	PCE (%)	AVT (%)	Ref.
PTB7-Th:IUIC	10.2	31.0	17
PTB7-Th:PC71BM	8.52	26.2	18
PTB7-Th:ITVfIC	8.21	33.7	19
PBDTTT-E-T:IEICO	6.0	25.0	20
PM6:Y6	12.8	25.6	21
PTB7-Th:ACS8	10.4	36.1	22
PCE-10: BT-CIC:TT-FIC	8.0	44.2	23
PDTIDTBT:PCBM	6.1	55.0	24
PTB7-Th:IEICO-4F	10.8	29.5	25
PM6:Y6:$PC_{71}BM$	8.1	36.2	26
PCE-10:A078	10.8	45.7	27

PTB7-Th:FOIC:$PC_{71}BM$	8.66	50.4	28
PTB7-Th:IDTBR	6.32	35.4	29
PTB7-Th:IEICO-4F	7.34	25.6	30
PBT1-C-2Cl:Y6	9.1	40.0	31
PTB7-Th:T2-ORH	6.93	34.0	32
PL-Cl:F8IC	11.0	35.0	33
PCE10-2Cl:IT-4F	8.25	33.0	34
PCE10-BDT2F:Y6	10.66	41.1	35
PM6:Y6	9.7	42.8	36
PM2:Y6-BO	6.3	40.0	37
P3HT:PCBM	2.9	45.0	38
PM6:Y6	7.46	36.4	39
D18-Cl: Y6:$PC_{71}BM$	11.58	25.5	40
PTB7-Th:ATT-9	9.37	35.5	41
PTB7-Th:PCDTBT: IEICO-4Cl	6.30	43.9	42
PM6:Hydrated BCF:Y6	8.3	33.7	43
PM6/BTP-eC9	13.1	27.8	This work

References

1 M. S. Su, C. Y. Kuo, M. C. Yuan, U. S. Jeng, C. J. Su and K. H. Wei, *Adv Mater*, 2011, **23**, 3315-3319.

2 Y. Cui, S. Zhang, N. Liang, J. Kong, C. Yang, H. Yao, L. Ma and J. Hou, *Adv. Mater.*, 2018, **30**, 1802499.

3 L. Arunagiri, G. Zhang, H. Hu, H. Yao, K. Zhang, Y. Li, P. C. Y. Chow, H. Ade and H. Yan, *Adv. Funct. Mater.*, 2019, **29**, 1902478.

4 L. Ye, Y. Xiong, Z. Chen, Q. Zhang, Z. Fei, R. Henry, M. Heeney, B. T. O'Connor, W. You and H. Ade, *Adv. Mater.*, 2019, **31**, 1808153.

5 M. Ren, G. Zhang, Z. Chen, J. Xiao, X. Jiao, Y. Zou, H. L. Yip and Y. Cao, *ACS Appl. Mater. Interfaces*, 2020, **12**, 13077-13086.

6 J. Wan, L. Zhang, Q. He, S. Liu, B. Huang, L. Hu, W. Zhou and Y. Chen, *Adv. Funct. Mater.*, 2020, **30**, 1909760.

7 R. Sun, Q. Wu, J. Guo, T. Wang, Y. Wu, B. Qiu, Z. Luo, W. Yang, Z. Hu, J. Guo, M. Shi, C. Yang, F. Huang, Y. Li and J. Min, *Joule*, 2020, **4**, 407-419.

8 K. Weng, L. Ye, L. Zhu, J. Xu, J. Zhou, X. Feng, G. Lu, S. Tan, F. Liu and Y. Sun, *Nat. Commun.*, 2020, **11**, 2855-2864.

9 Q. Li, L.-M. Wang, S. Liu, L. Guo, S. Dong, G. Ma, Z. Cao, X. Zhan, X. Gu, T. Zhu, Y.-P. Cai and F. Huang, *ACS Energy Lett.*, 2020, **5**, 3637-3646.

10 X. Wang, L. Zhang, L. Hu, Z. Xie, H. Mao, L. Tan, Y. Zhang and Y. Chen, *Adv. Funct. Mater.*, 2021, **31**, 2102291.

11 H. Ning, Q. Jiang, P. Han, M. Lin, G. Zhang, J. Chen, H. Chen, S. Zeng, J. Gao, J. Liu, F. He and Q. Wu, *Energy Environ. Sci.*, 2021, **14**, 5919-5928.

12 Y. Zhang, K. Liu, J. Huang, X. Xia, J. Cao, G. Zhao, P. W. K. Fong, Y. Zhu, F. Yan, Y. Yang, X. Lu and G. Li, *Nat. Commun.*, 2021, **12**, 4815-4828.

13 H. Chen, T. Zhao, L. Li, P. Tan, H. Lai, Y. Zhu, X. Lai, L. Han, N. Zheng, L. Guo and F. He, *Adv. Mater.*, 2021, **33**, 2102778.

14 L. Zhan, S. Li, X. Xia, Y. Li, X. Lu, L. Zuo, M. Shi and H. Chen, *Adv. Mater.*, 2021, **33**, 2007231.

15 X. Xu, L. Yu, H. Meng, L. Dai, H. Yan, R. Li and Q. Peng, *Adv. Funct. Mater.*, 2021, **32**, 2108797.

16 J. Wan, L. Zeng, X. Liao, Z. Chen, S. Liu, P. Zhu, H. Zhu and Y. Chen, *Adv. Funct. Mater.*, 2021, **32**, 2107567.

17 B. Jia, S. Dai, Z. Ke, C. Yan, W. Ma and X. Zhan, *Chem. Mater.*, 2017, **30**, 239-245.

18 B. Dudem, J. W. Jung, J. S. Yu, *J. Mater. Chem. A*, 2018, **6**, 14769-14779.

19 H. Huang, X. Li, L. Zhong, B. Qiu, Y. Yang, Z.-G. Zhang, Z. Zhang and Y. Li, *J. Mater. Chem. A*, 2018, **6**, 4670-4677.

20 C. Sun, R. Xia, H. Shi, H. Yao, X. Liu, J. Hou, F. Huang, H.-L. Yip and Y. Cao, *Joule*, 2018, **2**, 1816-1826.

21 Y. Bai, C. Zhao, X. Chen, S. Zhang, S. Zhang, T. Hayat, A. Alsaedi, Z. a. Tan, J. Hou and Y. Li, *J. Mater. Chem. A*, 2019, **7**, 15887-15894.

22 J. Chen, G. D. Li, Q. L. Zhu, X. Guo, Q. P. Fan, W. Ma and M. J. Zhang, *J. Mater. Chem. A*, 2019, **7**, 3745-3751.

23 Y. Li, C. Ji, Y. Qu, X. Huang, S. Hou, C. Z. Li, L. S. Liao, L. J. Guo and S. R. Forrest, *Adv. Mater.*, 2019, **31**, 1903173.

24 M. M. Tavakoli, R. Po, G. Bianchi, A. Cominetti, C. Carbonera, N. Camaioni, F. Tinti and J. Kong, *PNAS*, 2019, **116**, 22037-22043.

25 R. Xia, C. J. Brabec, H.-L. Yip and Y. Cao, *Joule*, 2019, **3**, 2241-2254.

26 B. H. Jiang, H. E. Lee, J. H. Lu, T. H. Tsai, T. S. Shieh, R. J. Jeng and C. P. Chen, *ACS Appl Mater Interfaces.*, 2020, **12**, 39496-39504.

27 Y. Li, X. Guo, Z. Peng, B. Qu, H. Yan, H. Ade, M. Zhang and S. R. Forrest, *PNAS*, 2020, **117**, 21147-21154.

28 Q. Liu, L. G. Gerling, F. Bernal-Texca, J. Toudert, T. Li, X. Zhan and J. Martorell, *Adv. Energy Mater.*, 2020, **10**, 1904196.

29 H. Park, J. H. Lee, S. Lee, S. Y. Jeong, J. W. Choi, C. L. Lee, J. H. Kim and K. Lee, *ACS Appl Mater Interfaces.*, 2020, **12**, 2276-2284.

30 S. Song, H. W. Cho, J. Jeong, Y. J. Yoon, S. Y. Park, S. Song, B. H. Woo, Y. C. Jun, B. Walker and J. Y. Kim, *Solar RRL*, 2020, **4**, 2000201

31 Y. Xie, Y. Cai, L. Zhu, R. Xia, L. Ye, X. Feng, H. L. Yip, F. Liu, G. Lu, S. Tan and Y. Sun, *Adv. Funct. Mater.*, 2020, **30**, 2002181.

32 N. G. An, T. Lee, J. Heo, J. W. Kim, S. Song, W. Lee, B. Walker, E. Lim and J. Y. Kim, *Solar RRL*, 2021, **5**, 2000742.

33 Y. Chang, X. Zhu, L. Zhu, Y. Wang, C. Yang, X. Gu, Y. Zhang, J. Zhang, K. Lu, X. Sun and Z. Wei, *Nano Energy*, 2021, **86**, 106098.

34 X. Huang, J. Oh, Y. Cheng, B. Huang, S. Ding, Q. He, F. Wu, C. Yang, L. Chen and Y. Chen, *J. Mater. Chem. A*, 2021, **9**, 5711-5719.

35 X. Huang, L. Zhang, Y. Cheng, J. Oh, C. Li, B. Huang, L. Zhao, J. Deng, Y. Zhang, Z. Liu, F. Wu, X. Hu, C. Yang, L. Chen and Y. Chen, *Adv. Funct. Mater.*, 2021, **32**, 2108634.

36 H. I. Jeong, S. Biswas, S. C. Yoon, S. J. Ko, H. Kim and H. Choi, *Adv. Energy Mater.*, 2021, **11**, 2003576.

37 T. Jiang, G. Zhang, R. Xia, J. Huang, X. Li, M. Wang, H. L. Yip and Y. Cao, *Mater. Today Energy.*, 2021, **21**, 100807.

38 S. Wageh, M. Raïssi, T. Berthelot, A. A. Al-Ghamdi, A. M. Abusorrah, W. Boukhili and O. A. Al-Hartomy, *Adv. Eng. Mater.*, 2021, **23**, 2001305.

39 N. Yao, Y. Xia, Y. Liu, S. Chen, M. P. Jonsson and F. Zhang, *ACS Appl. Energy Mater.*, 2021, **4**, 14335-14341.

40 S. Han, Z. Bu, Q. Zhang, X. Zhang, C. Liu and W. Guo, *ACS Sustain. Chem. Eng.*, 2022, **10**, 2241-2247.

41 W. Liu, S. Sun, S. Xu, H. Zhang, Y. Zheng, Z. Wei and X. Zhu, *Adv. Mater.*, 2022, https://doi.org/10.1002/adma.202200337.

42 H. Tang, Y. Li, H. Liu, J. Wu, L. Chen, Y. Fu and Z. Xie, *J. Mater. Chem. C*, 2022, **10**, 3720-3728.

43 Y. Tang, H. Zheng, X. Zhou, Z. Tang, W. Ma and H. Yan, *Small Methods*, 2022, **6**, 2101570.